Paper ID ICLASS06-281
HYPOBARIC PRESSURE EFFECTS ON R-134a COOLING SPRAYS FOR LASER DERMATOLOGY

Henry Vu [1], Walfre Franco [2], Wangcun Jia [3] and Guillermo Aguilar [4]

[1]Department of Mechanical Engineering, University of California, Riverside, CA 92507 USA, hvu@engr.ucr.edu
[2]Beckman Laser Institute, University of California, Irvine, CA 92617 USA, wfranco@uci.edu
[3]Beckman Laser Institute, University of California, Irvine, CA 92617 USA, wjia@uci.edu
[4]Department of Mechanical Engineering, University of California, Riverside, CA 92507 USA, gaguilar@engr.ucr.edu

ABSTRACT R-134a sprays have been widely used as a method to protect the epidermis during laser therapies of hyper-vascular lesions, such as port wine stains, due to their high heat flux and precise control of cooling duration. Recent studies have shown that the use of vacuum cups during laser treatment can physically dilate the vasculature of interest and improve therapeutic outcome. However, the effects of these vacuum pressures on the cooling sprays remains unknown. In this paper, characteristics of steady-state and transient R-134a sprays, measured with a Phase Doppler Particle Analyzer (PDPA) at different pressures are presented. Ambient pressure changes from 0 to -50 kPa result in significant droplet size reductions while simultaneously increasing droplet velocities. The combined results is a slight increase in inertial Weber numbers for most conditions and a decrease in liquid volume flux. These changes appear to occur mainly during primary and secondary atomization of the spray at distances within beyond 30 mm from the nozzle tip. Hypobaric pressures appear to have little effect on droplet evaporation in flight beyond 30mm. The resulting implications for transient heat transfer in a skin phantom model is also discussed.

Keywords: flashing jet, refrigerant spray, transient cooling

1. INTRODUCTION

Laser treatment of various hypervascular dermatoses, particularly port wine stains, has become common practice in recent years[1, 2]. Laser light of an appropriate wavelength (585 nm) is used because it is highly absorbed by the target chromophore, hemoglobin, within the vasculature. This absorption of energy induces the desired thermal necrosis of the hypervascular lesions. However, melanin within the epidermis also absorbs a wide spectrum of light energy. To avoid epidermal injury by heating, a method of precooling using a short duration refrigerant spray has found widespread acceptance because of the high heat fluxes possible and precise control of cooling duration[3]. Thus, rapid and spatially selective cooling of the epidermis is possible without lowering the temperature of the deeper-seated target chromophores. With precooling, the epidermis is kept below the damage threshold during heating of the tissue by the subsequent laser pulse.

Despite the effectiveness of this epidermal protection technique, complete blanching of the lesions is rarely achieved. Darker-skinned patients also normally cannot be treated due to higher melanin absorption. Treatment effectiveness could potentially be improved by increasing laser fluence, but this is limited by the epidermal protection that the sprays can provide. Additionally, the sprays have been found to induce highly non-uniform cooling[4], potentially leading to uneven protection and skin dyspigmentation or scarring. Many studies have been done to characterize these refrigerant sprays and their accompanying heat transfer[5-8], but the mechanisms of atomization and heat transfer are still not well understood.

Recently, a new treatment technique using vacuum suction cups to dilate the blood vessels and increase blood volume fraction prior to laser treatment has shown promising results[9, 10]. Improved blanching with the same radiant exposure is possible. As air is evacuated from these suction cups, air pressure is reduced. From Figure 1, it is known that the properties of R-134a are a strong function of pressure, but the effects of hypobaric pressures on the spray itself have not been quantitatively identified. Therefore, the purpose of this study is to quantitatively characterize the spray and observe the changes due to varying ambient pressure. Explanations for the observed changes will be given, along with implications on heat transfer.

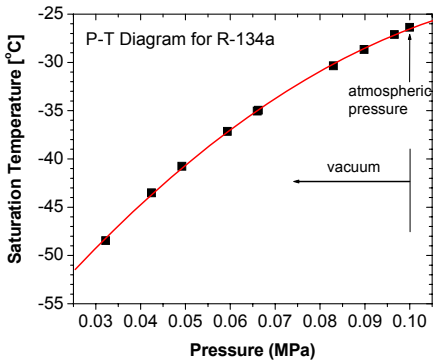

Figure 1: Thermodynamic properties of R-134a.

2. EXPERIMENTAL METHODS

2.1 Spray system

The liquid refrigerant used was R-134a (1,1,1,2-tetrafluoroethane; National Refrigerants, Philadelphia, PA) which was maintained at saturation pressure 627 kPa at room temperature) in a standard 30 lb bottle.

The refrigerant was delivered via a high pressure hose to a clinically-used miniature solenoid valve and nozzle (GentleLASE^{TM}; Candela, Wayland, MA). The nozzle was a stainless steel plain circular orifice tube of 0.55 mm inner diameter and approximately 38 mm length. There was a 29° bend in the nozzle at its midpoint, but the nozzle exit was oriented to deliver vertical, downward-oriented sprays. Axial positions, *z*, were defined as the vertical distances between the nozzle exit tip and the probe measurement volume. The solenoid valve and nozzle were kept centered with respect to the measurement point and displaced using a translational positioning system to desired *z* spanning 15 to 90 mm with 15 mm increments. In clinical practice, *z* is normally fixed at 30 mm so this study includes the clinically relevant distance. Additionally, the spray was also displaced to radial locations, *r*, in 1mm increments with z fixed at 30mm to observe the hypobaric pressure effects on radial characteristics of the spray.

2.2 Spray Characterization

Spray droplet velocity and diameter were measured using a Phase Doppler Particle Analyzer (PDPA; TSI Incorporated, Shoreview, MN) with an Argon ion laser emitting 488 and 514.5 nm wavelength light beams. A schematic of this setup is shown in Figure 1. This system was capable of measuring velocity along two perpendicular axes, but only the axial velocities will be presented since the magnitudes of the lateral (radial) velocities and their data rates were significantly smaller. All steady-state PDPA diameter and velocity values were averages of a minimum of 10000 measurement points taken from steady-state sprays. According to Tate and Marshall [11], this corresponds to an error in cumulative distribution of less than 1.4%. D_{10} averaging of diameter was used because it is a first-order expression and, therefore, less sensitive to measurement errors. Errors in velocity are estimated to be less than 1% according to an analysis by Yanta [12].

Sprays in the transient state were studied using a 30 ms duration spurt, which is typical in clinical practice. Averages of velocity and diameter were taken of 1 ms time bins throughout the duration of the spray in order to observe dynamic changes in spray characteristics. Approximately 40 spurts were used to obtain a minimum of 100 data points for each time bin, though most bins were averages of 1000 or more points. This corresponds to maximum errors in diameter and velocity of 13% and 6%, respectively.

2.3 Pressure Control

In order to control the ambient pressure of the environment surrounding the nozzle, a custom clear acrylic chamber was designed and fabricated to enclose the spray system. The chamber walls were 12 mm thick to withstand the vacuum pressures needed for the study. The walls were also designed to be perpendicular to the paths of incident and scattered light to minimize refraction. The walls were found to decrease laser power by about 15%. Focal length of the laser was also lengthened slightly so the receiving probe position was adjusted to compensate for this. Changes in diameter and velocity due to the chamber walls was considered to be negligible. Gauge pressures for the study were 0, -17, -35, and -50 kPa and

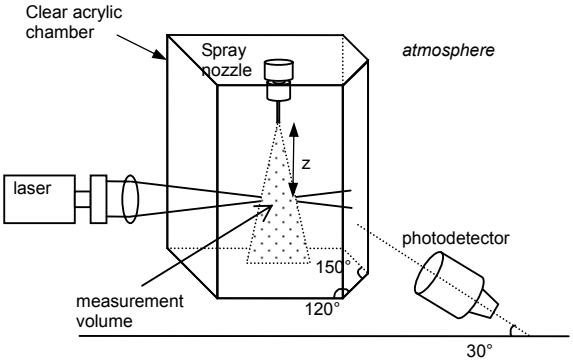

Figure 2. A schematic of the PDPA system and clear acrylic chamber.

obtained using the building vacuum system. After each measurement, the chamber was flushed with dry air in order to prevent refrigerant vapor build-up. Relative humidity within the chamber was maintained between 11-15% for all experiments.

2.4 Heat Transfer Measurement

Spray heat transfer was assessed using a custom-designed sensor consisting of a 4.5 x 6.5 x 7 mm thick epoxy block (RBC 3100, RBC Industries, Warwick, RI) with a fast-response flat thermocouple (CO2-K, Omega Engineering, Stamford, CT) embedded at the top surface. Epoxy was used as the substrate because its thermal properties are similar to human skin [13] (see Table 1). A 4000 Hz data rate was used for all measurements. From previous studies, the heat transfer can be assumed to be one-dimensional. Taking the measured temperature as the surface temperature of the substrate, Duhamel's theorem may then be used to obtain the one-dimensional temperature distribution within the substrate [19]:

$$T(x,t) = T_o + \int_{t_o}^{t} u(x,t-\lambda)\frac{dT_s(\lambda)}{d\lambda}d\lambda + \sum_{i=0}^{N-1} u(x,t-\lambda_i)\Delta T_{s,i} \quad (1)$$

where T_o is the initial temperature assumed to be uniform over the entire substrate, $u(x,t)$ is the unit step temperature response function, λ is the time step, N is the total number of time steps, and $T_s(t)$ the known surface temperature as a function of time. The integral portion of Equation 1 allows for a continuous surface temperature and the summation portion allows for N discontinuous steps in temperature. This equation permits the determination of the temperature distribution within the substrate based on known $T_s(t)$ but is limited to linear problems with constant thermal properties. For a semi-infinite planar solid, the unit step

Table 1. Epoxy versus human dermis thermal properties.

	Epoxy	Dermis
k [W/m K]	0.217	0.54
ρ [kg/m3]	1160-1400	1150
c [J/kg K]	1.22x10-7	1.26x10-7

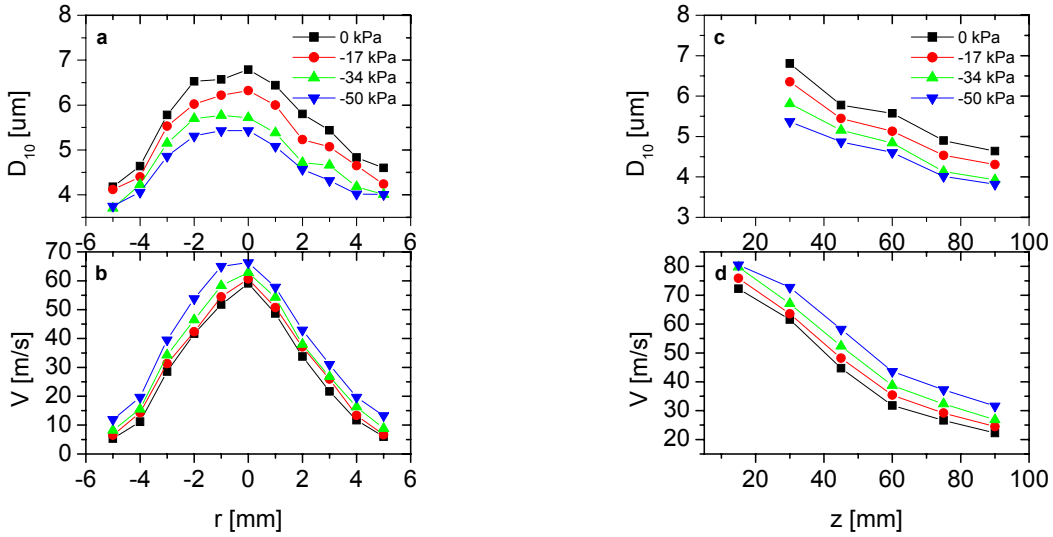

Figure 3. Hypobaric pressure effects of D_{10} and V for various z and r.

function is:

$$u(x,t) = 1 - erf\left(\frac{x}{2\sqrt{\alpha t}}\right) \quad (2)$$

For continuous $T_s(t)$, surface heat flux, q, can be determined by Fourier's law and differentiating Equation 1:

$$q(t) = -k\left.\frac{\partial T}{\partial x}\right|_{x=0} = -k\int_{t_o}^{t}\left.\frac{\partial u(x,t-\lambda)}{\partial x}\right|_{x=0} T_s'(\lambda)d\lambda \quad (3)$$

and substituting Equation 2, the expression for q simplifies to:

$$q(t) = \sqrt{\frac{k\rho c}{\pi}}\int_{t_o}^{t}\frac{T_s'(\lambda)}{\sqrt{t-\lambda}}d\lambda \quad (4)$$

If the surface temperature is measured at discrete times and is assumed to change linearly within each time step a convenient approximate analytical solution to Equation 4 is:

$$\hat{q}(t) = 2\sqrt{\frac{k\rho c}{\pi}}\sum_{i=1}^{M}\frac{T_{s,i} - T_{s,i-1}}{\sqrt{t_M - t_i} + \sqrt{t_M - t_{i-1}}} \quad (5)$$

This equation is thus employed to obtain a direct solution for the surface q experienced by the substrate.

2.5 Droplet Weber Number Calculation

Weber numbers, defined generally as:

$$We = \frac{\rho v^2 D}{\sigma} \quad (6)$$

were calculated from the above PDPA measurements. Two forms of Weber number are actually in use, and they provide information about different aspects of the spray. Their difference lies in what medium is used for density, the dispersed fluid composing the droplet (R-134a) or the surrounding continuous fluid (air/vapor).

The former, denoted We_d in this study, provides the ratio of droplet inertial forces to droplet surface tension forces and is typically used in heat transfer studies[7, 14-16]. The latter, We_a, is the ratio of aerodynamic forces to droplet surface tension and is a measure of droplet stability or likelihood of breaking up in flight due to drag forces with the surround medium [17-19]. Droplets are generally assumed to be stable below critical values of between 10-20 [18]. The density and surface tension of R-134a were assumed to be constant values of 1234 kg/m^3 and 0.0079 N/m, respectively. The density of the surrounding medium was assumed to be that of pure air, and a function of the absolute pressure within the chamber.

2.6 Volume Flux Calculation

Volume fluxes of the spray can be calculated from PDPA-measured characteristics using an algorithm supplied by TSI, Incorporated. Only axial fluxes are considered since radial velocities were significantly smaller. Volume flux is defined as flow rate (cm^3/s) of liquid spray droplets per unit area (cm^2). It is calculated as the sum of the fluxes of discrete size bins. The flux of each individual size bin is determined by multiplying its volume fraction by its mean velocity.

The volume fraction for the jth size bin is expressed as

$$L_j = \frac{\frac{\pi}{6}\sum D_j^3 t_j}{V_{probe\_j}\, t_{tot}} \quad (7)$$

where summation is done for all the particle diameters D_j and their transit times t_j in the jth size bin. t_{tot} represents the total measurement time and V_{probe_j} is the volume of the probe region for the jth size bin.

It is known that the effective volume of the probe region increases with the increasing particle diameter, due to increasing signal strength. The following definition of V_{probe_j} provides a measure of the size dependency of the probe region on the particle size:

$$V_{probe\_j} = \left(\frac{s\, f_{rf}}{f_{rb}\sin\phi}\right) W_j\, h_j \quad (8)$$

where s, f_{rf}, f_{rb} and ϕ are the slit width, focal length of the front receiver lens, focal length of the back receiver lens and the collection (off-axis) angle respectively. The term in the parentheses represents the length of the probe

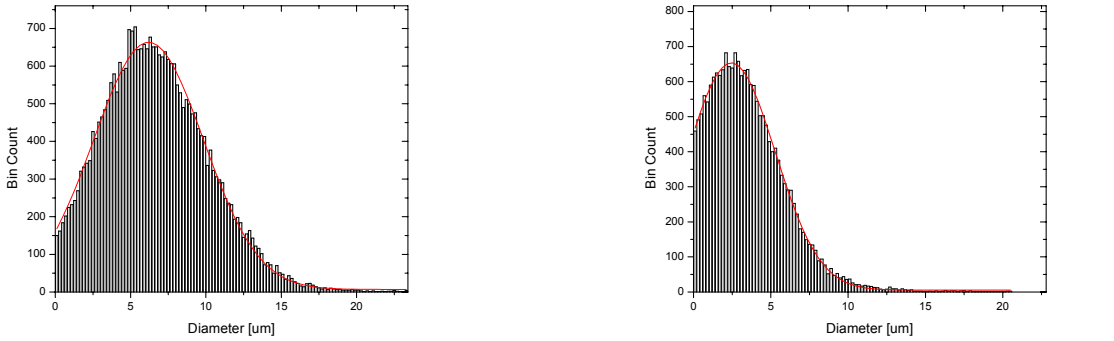

a **b**

Figure 4. Histogram data for diameter along with Gaussian fits for a) z=30mm, P=0 kPa and b) z=90mm, P=-50 kPa.

region, whereas W_j and h_j are the size-dependent width and
height of the probe region. W_j is the smaller of either the largest path length for the jth size bin or the probe volume width determined by the intensity limits. Particle path lengths are the product of the particle velocity and the transit time. h_j is the mean path length for the jth size class. This algorithm does not consider the contribution to volume flux from non-validated signals so large errors may results with low validation rates.

3. RESULTS AND DISCUSSION

3.1 Steady-State Sprays

Steady-state spray velocity and D_{10} measurements are presented in Figure 3. Generally, with decreasing pressure there is a simultaneous decrease in droplet size and increase in velocity. Due to the high density of the spray at z=15mm, diameter measurements at that point were prone to errors and thus are not shown. Radial measurements at z=30mm show symmetric, bell-shaped distributions in both velocity and D_{10}. The diameter profile of Figure 3a indicates that the spray is generally better atomized near the cone edge so the nozzle walls may be contributing to the atomization process during or immediately proceeding internal flow. The slight asymmetry in diameter with radial location is possibly due to the influence of valve or nozzle irregularities in interior surface roughness or the shape of the orifice. For velocity, the radial symmetry is more apparent and at z=30mm, it steeply decreases from 60 m/s to nearly 0 m/s. This profile may, again, stem from the velocity profile of internal flow within the nozzle. These profiles are a function of the device used, but for some other full-cone sprays, velocity and diameter profiles are often assumed to be uniform and only a function of z [14, 20].

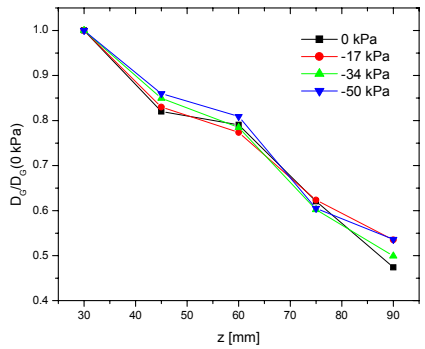

Figure 5. Non-dimensional evaporation rates as a function of z.

Figure 3c shows D_{10} decreasing with respect to z. Droplet diameter evolution with z can be used to determine evaporation rate. Measured diameters are very small, however, so many droplets may be evaporating below the threshold of detection or evaporating completely, which would skew the population distribution to larger droplets. In order to assess this effect, droplet size histograms are presented in Figure 4 using size bins of 0.2 um. Gaussian distributions are apparent for all z locations and pressures, but, indeed they appear to be cut off on the lower end. As droplet sizes continue to get smaller with increasing z or decreasing pressure, these distributions will shift more to the left. D_{10} averaging of the measurable droplet populations is thus not appropriate for assessing changes in evaporation rate. In order to accomplish this, Gaussian fits of the droplet distributions were calculated and the diameters corresponding to the maximums of the distributions were used to represent the entire population. This eliminates the increasing influence that the larger droplets have on the representative diameter. The ratio of these Gaussian peak diameters (D_G) with D_G at z=30mm are plotted as a function of z in Figure 5. Because the curves for different pressures nearly coincide, pressure has little effect on the droplet evaporation relative to diameters at z=30mm. This means that pressure decreases droplet diameter before z=30mm through primary and secondary atomization. Once stable droplets have been formed, the decrease in pressure has little effect on the evaporation rate from the droplet.

On the other hand, droplet velocity populations remained well within the detection limits of the system. Therefore, simple linear fits of velocity data in Figure 3d and extrapolations to z=0mm for each pressure provide an estimation for changes in exit velocity and acceleration. Slopes, y-intercepts, and correlation coefficients are indicated in Table 2. This information shows that ambient pressure has a large influence on nozzle exit velocity (V_o) but an insignificant effect on the acceleration or rate of change of droplet velocity in flight (A). These exit

Table 2. Linear Regression fits of velocity as a function of z.

	$V_{meas}=V_o-Az$						
P [kPa]	**V_o [m/s]**	**A_V**	**Correlation (R)**	**V_L [m/s]**	**V_T [m/s]**	**C_L**	**C_T**
0	80	0.70	0.976	28.5	39.0	2.81	2.05
-17	83	0.71	0.981	29.0	39.6	2.88	2.1
-34	88	0.73	0.984	29.4	40.3	2.98	2.18
-50	91	0.70	0.986	29.8	40.9	3.04	2.22

velocities can be compared to theoretical pipe flow velocities for both laminar and turbulent flow:

$$V_L = \left(\frac{2\Delta P}{\rho_l}\right)^{0.5} \quad (9)$$

$$V_T = \left(\frac{\Delta P D_N}{2\rho_l L_N C_f}\right)^{0.5} \quad (10)$$

$$C_f = 0.079\,\mathrm{Re}_N^{-0.25} \quad (11)$$

$$V_0 = C_{L,T} \cdot V_{L,T} \quad (12)$$

The Blasius equation is used to determine C_f in turbulent flow.

Results show that extrapolated effluent velocities are much higher than those predicted theoretically. Additionally, multiplicative constants relating theoretical to actual velocities (Equation 12) actually increase as pressures decrease. This shows that the discrepancy increases with decreasing pressure. Because of the thermodynamic instability of the fluid as it undergoes the pressure drop across the valve, one explanation for this discrepancy is the acceleration of the fluid within the nozzle due to flash evaporation. This flash evaporation would intensify as the pressure drop increases from the applied vacuum.

We_d and We_a values were also calculated using D_{10} and velocity measurements. Figure 6 shows that the combined effect of velocity and D_{10} changes is an increase in We_d values as ambient pressures decrease. It is well known that heat flux from sprays can be correlated with We_d [14, 15] and this, in fact, has been done for dermatological cooling studies [7]. Higher We_d droplets are more capable of penetrating the liquid film that forms at the surface of the cooling surface and can thereby increase the intensity of heat extraction.

We_a values were all found to be below critical, ranging from 5.5 to 0.5. For brevity, these values are not graphed. This indicates that droplets are stable and spherical at z=30mm and beyond. The change in droplet sizes beyond z=30mm is likely only due to droplet evaporation, not secondary atomization from shearing forces with the surrounding air. The fine atomization of the spray resulting from a simple plain-orifice nozzle would suggest that the spray atomization mechanisms of R-134a are significantly thermodynamic in nature and not only hydrodynamic as is the case for many other cooling sprays. The thermodynamic instability of the refrigerant due to the sudden and large pressure drop may induce a flash boiling event within the nozzle and/or immediately at the nozzle exit [21]. This violent expansion of the fluid would cause it to break up immediately into fine droplets.

The influence that vacuum has on the liquid volume flux of the spray has important implications for heat transfer. Calculated values ranged from 0.0032-0.011 cc/cm^2/s. However, due to the sensitivity of the algorithm to the changes in PDPA size validation rate with different z, the volume fluxes at different z are not comparable. Volume fluxes are, however, still meaningful if presented as a ratio with volume flux at 0 kPa for each respective z as shown in Figure 7. The curves indicate that with decreasing pressure, volume fluxes also decrease. Because

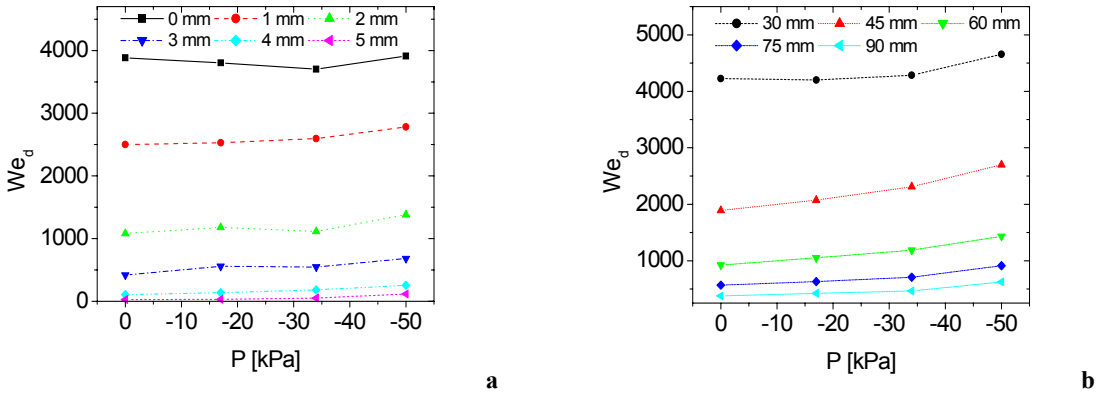

Figure 6. Hypobaric pressure effects on spray droplet We_d for a) radial locations at z=30mm and b) axial locations at r=0mm.

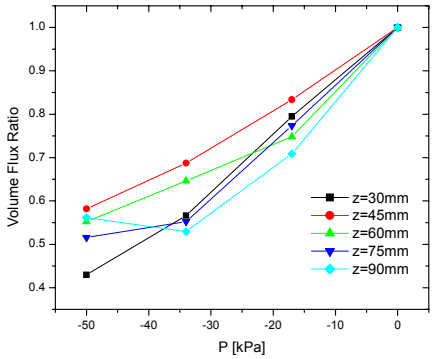

Figure 7. Volume flux ratio as a function of pressure.

the change in evaporation rate has been found to be small, the volume flux decrease can be explained by an increase in spray cone angle and spray area as determined in a previous study [9]. Droplet density decreases as spray area increases and thus volume flux decreases.

3.2 Transient Sprays

Because of the short durations of these sprays in clinical application, it is useful to examine the characteristics of the spray in the transient state. Calculated We_d numbers based on time bin-averaged diameter and velocity for a 30 ms spurt at z=30mm provide a measure of the transient nature of the spray. It is evident from Figure 8 that there are three zones of a transient spray: developing, steady, and terminating zones. In zones I and III, We_d will go through abrupt changes, but remain fairly steady in zone II at values similar to those measured for a steady-state spray. We_d dependence on pressure is likewise similar to steady-state sprays by either staying the same or increasing with decreasing pressure. Zone I is characterized by high We_d that quickly decrease to steady state values. Generally in Zone III, there is a gradual decrease in We_d, though We_d actually increases first before decreasing for -34 kPa and -50 kPa at r=0mm.

3.3 Transient Heat Transfer

Measured temperature and heat flux changes due to 30 ms spurts at z=30mm are shown in Figure 9. q values show a decrease in maximum value and a time delay in reaching maximum with decrease in ambient pressure. Transient spray heat transfer is a complex function of droplet We_d, droplet temperature, and volume flux among other variables. The applied vacuum pressure affects these variables to different degrees. Though droplet temperatures have not been evaluated in this study, We_d numbers have been shown to remain the same or increase slightly with decreasing pressure. Volume flux has also been shown to decrease. Transient We_d and q plotted together in Figure 10 show weak correlation. Generally, the initial We_d transients occur before maximum heat flux is reached and ending transients appear to have little influence on heat flux. At the spray conditions of this study, heat transfer is likely a stronger function of volume flux, as both are reduced concurrently with decreasing pressure. This can be explained by reasoning that it takes longer for the surface to become fully wetted, leading to less intense cooling. The volume flux of the initial few milliseconds of the spray is very important in determining the maximum heat flux and time to reach maximum. With reduced volume flux, the surface is likely only partially wetted for a longer period of time.

4. CONCLUSION

This work has shown through quantitative PDPA measurement the effects that hypobaric pressures up to -50 kPa have on R-134a refrigerant cooling sprays. A D_{10} decrease and velocity increase were observed in both the axial and radial cross-sections of the spray cone. A novel technique using Gaussian fitting was used to assess the evaporate rate of very small droplets. Hypobaric pressures were shown to have little effect on the rate of change of velocity and evaporation at z≥30mm. The combined effect was generally a small increase in We_d. We_a ranged from 5.5 to 0.5 and were well below critical values at locations z≥30mm. Significant relative decreases in liquid volume fluxes were also observed for all z locations. 30ms spurts were characterized by short initial and ending transients with steady-state regions exhibiting We_d similar to those of steady-state sprays. Maximum q was measured to decrease, accompanied by a delay in reaching maximum as pressures decreased. There was little correlation, however, between in transient We_d and transient heat transfer. Decreases in q more likely result from volume flux decreases.

Further studies are necessary to evaluate the effects of hypobaric pressures on the primary and atomization

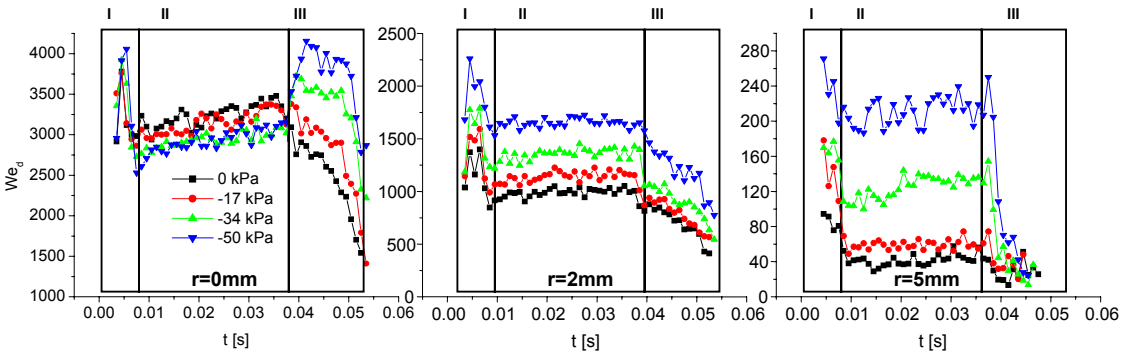

Figure 8. Transient zones for a 30 ms spurt at z=30mm.

mechanisms of the spray, specifically flash evaporation at locations near the nozzle exit and within the nozzle.

5. NOMENCLATURE

c	specific heat capacity	[J/kg/K]
C_f	coefficient of drag	
C	multiplicative constant for velocity	
D	droplet diameter	[um]
D_G	Gaussian peak diameter	[um]
D_N	nozzle diameter	[mm]
D_{10}	arithmetic average droplet diameter	[um]

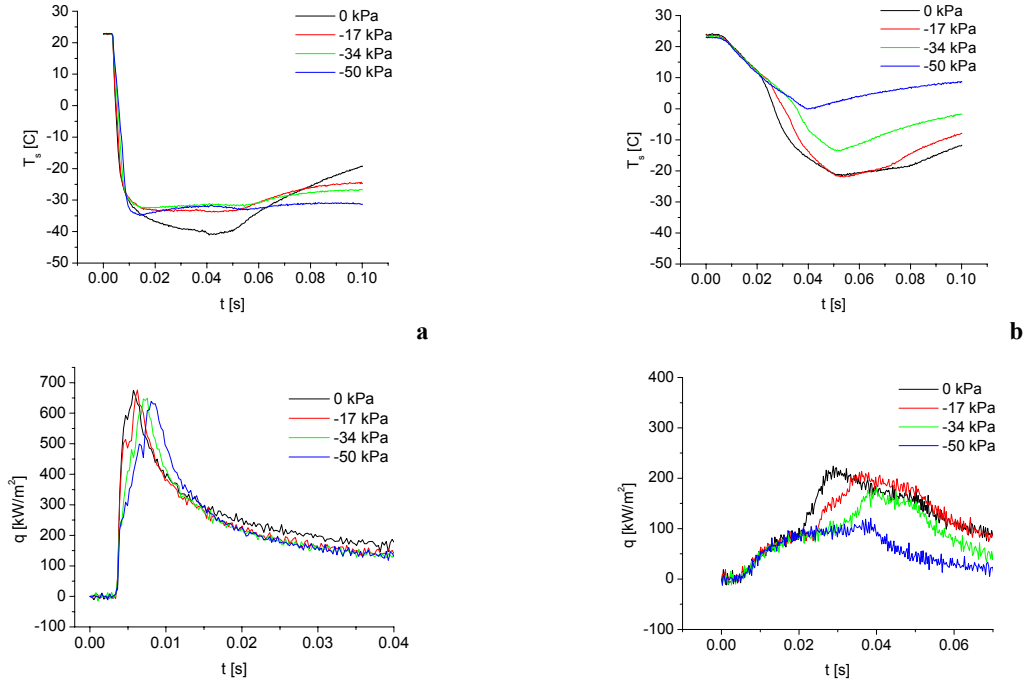

Figure 9. Measured T_s for a) r=0mm and b) r=5mm and q for c) r=0mm and d) r=5mm from a 30 ms spurt at z=30mm.

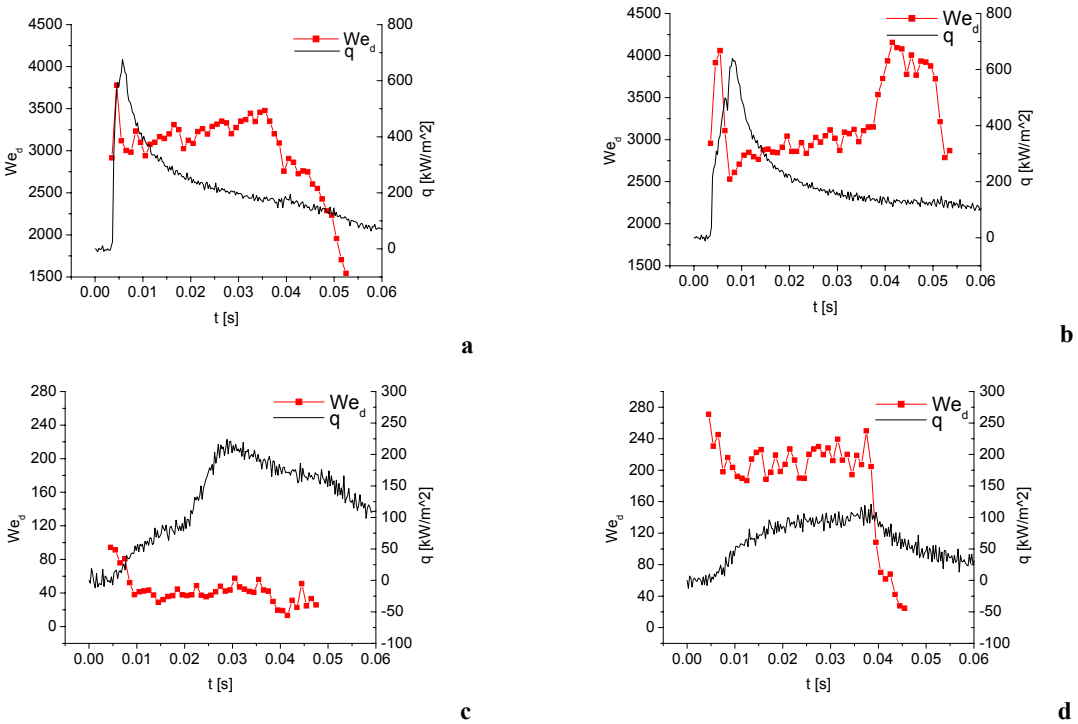

Figure 10. Transient We_d superimposed with transient q for a) r=0mm, P=0kPa b) r=0mm, P=-50kPa c) r=5mm, P=0kPa d) r=5mm, P=-50kPa from a 30 ms spurt at z=30mm.

h	height of probe volume	[cm]
k	thermal conductivity	[W/m/K]
f_{rf}	focal length of front receiver lens	[cm]
f_{rb}	focal length of back receiver lens	[cm]
L	volume fraction	
L_N	nozzle length	[mm]
P	pressure	kPa
$q(t)$	heat flux	[kW/m^2]
Re	Reynolds number	
r	radial distance from center of spray	[mm]
s	slit width	[cm]
T_o	initial substrate temperature	[°C]
T_s	substrate surface temperature	[°C]
$T(x,t)$	substrate temperature	[°C]
$u(x,t)$	unit step function for semi-infinite planar solid	
V	velocity	[m/s]
V_L	laminar pipe velocity	[m/s]
V_T	turbulent pipe velocity	[m/s]
V_{probe}	measurement probe volume	[cm^3]
W	width of probe volume	[cm]
We_d	inertial Weber number	
We_a	aerodynamic Weber number	
z	axial distance from nozzle exit	[mm]
ρ	density	[kg/m$^{3]}$
σ	surface tension	[N/m]
ϕ	receiver off-axis angle	

6. REFERENCES

1. Nelson J.S., Milner T.E., Anvari B., Tanenbaum B.S., Kimel S., Svaasand L.O., Jacques S.L., Dynamic epidermal cooling during pulsed laser treatment of port wine stain. A new methodology with preliminary clinical evaluation. Arch. Dermatol., Vol. 131, pp. 695-700, 1995.

2. Torres J.H., Nelson J.S., Tanenbaum B.S., Milner T.E., et al., Estimation of internal skin temperatures in response to cryogen spray cooling: Implications for laser therapy of port wine stains. IEEE J. Selected Topics Quantum Electron., Vol. 5, pp. 1058-1066, 1999.

3. Verkruysee W., Majaron B., Tanenbaum B.S., Nelson J.S., Optimal cryogen spray cooling parameters for pulsed laser treatment of prot wine stains. Lasers in Surgery and Medicine, Vol. 27, pp. 165-170, 2000.

4. Franco W, Liu J., Wang G.X., Nelson J.S., Aguilar G., Radial and temporal variations in surface heat transfer during cryogen spray cooling. Phys Med Biol, Vol. 50, pp. 387-397, 2005.

5. Aguilar G., Majaron B., Verkruysee W., Zhou Y., Nelson J.S., Lavernia E.J., Theoretical and experimental analysis of droplet diameter, temperature, and evaporation rate evolution in cryogenic sprays. International Journal of Heat and Mass Transfer, Vol. 44, pp. 3201-3211, 2001.

6. Aguilar G., Majaron B., Verkruysee W., Nelson J.S., Lavernia E.J. Characterization of cryogenic spray nozzles with application to skin cooling. in Proceedings of IMECE 2000: The International Mechanical Engineering Congress and Exposition, 2000.

7. Pikkula B.M., Tunnell J.W., Anvari B, Methodology for characterizing heat removal mechanism in human skin during cryogen spray cooling. Annals of Biomedical Engineering, Vol. 31 pp. 493-504, 2004.

8. Pikkula B.M., Tunnell J.W., Change D.W., Anvari B., Effects of droplet velocity, diameter, and film height on removal during cryogen spray cooling. Annals of Biomedical Engineering, Vol. 32, pp. 1131-1140, 2004.

9. Aguilar G., Franco W., Liu J., Svaasand L.O., Effects of hypobaric pressure on human skin: Implications for cryogen spray cooling (Part II). Lasers in Surgery and Medicine, Vol. 36, pp. 130-135, 2005.

10. Aguilar G., Svaasand L.O., Nelson J.S., Effects of Hypobaric Pressure on Human Skin:Feasibility Study for Port Wine Stain Laser Therapy (Part I). Lasers in Surgery and Medicine, Vol. 36, pp. 124-129, 2005.

11. Tate R.W., Marshall W.R., Atomization by centrifugal pressure nozzles. Chemical Engineering Progress, Vol. 49, pp. 169-174, 1953.

12. Yanta W.J., Turbulence measurements with a laser doppler velocimeter., Naval Ordinance Laboratory, Rept. 73-94, White Oak, Silver Spring, MA, 1975.

13. Duck F.A., Physical properties of tissue: a comprehensive reference book, Academic Press, 1990.

14. Hsieh S.S., Fan T.C., Tsai H.H., Spray cooling characteristics of water and R-134a. Part I: nucleate boiling. International Journal of Heat and Mass Transfer, Vol. 47, pp. 5703-5712, 2004.

15. Hsieh SS, Fan T.C., Tsai H.H., Spray cooling characteristics of water and R-134a. Part II: transient cooling. International Journal of Heat and Mass Transfer, Vol. 47 pp. 5713-5724, 2004.

16. Incropera FP, DeWitt D.P., Fundamentals of Heat and Mass Transfer. 4th ed., John Wiley and Sons, 1996.

17. Hinze J., Fundamentals of the hydrodynamic mechanism of splitting in dispersion processes, AIChE, Vol. 1, pp. 289-295, 1955.

18. Lefebvre A., Atomization and Sprays, Hemisphere Pub. Corp., 1989

19. Ranger A., Nicholls J., Use of breakup time data and velocity history data to predict the maximum size of stable fragments for acceleration-induced breakup of a liquid drop. Int J Multiphase Flow, Vol. 13, pp. 741-757, 1969.

20. Ghodebane M., Holman J.P., Experimental study of spray cooling with Freon-113. Int J Heat Mass Transfer, Vol. 34, pp. 1163-1174, 1991.

21. Reitz R.D., A photographic study of flash-boiling atomization. Aerosol Science and Technology, Vol. 12, pp. 561-569, 1990.